Opportunities and Challenges of C+L Transmission Systems

Mattia Cantono, Rene Schmogrow, Matt Newland, Vijay Vusirikala, and Tad Hofmeister

(Invited Paper)

***Abstract*—C+L open line systems represent a cost-effective way to scale backbone network capacity. In this article, we review challenges and opportunities for C+L line systems stemming from Google's experience in designing, deploying, and operating a global C+L open optical network. We discuss business, operational, and technical aspects of C+L systems, and describe best practices for designing C+L links. Finally, we compare C and C+L systems, showing how the latter not only conceal capacity penalties but can even increase, depending on the deployed fiber types, the total system capacity with respect to two parallel C-band only systems.**

***Index Terms*—C+L systems, open line systems, wideband transmission.**

I. Introduction

GOOGLE'S backbone optical network is designed to provide connectivity to Google's datacenters for Internet and cloud computing services connecting billions of users globally. As Google's datacenter network capacity scaled by 100x over ten years to more than 1 Pbps of bisection bandwidth [1], the backbone network was required to scale as well. Over the last decade, Google's long-haul network has reached a global scale, and has grown dramatically by approximately two orders of magnitude in capacity [2]–[4].

Such growth has been enabled by the advancement of optical communication technologies [5] in particular the advent of transponders based on polarization multiplexed, multilevel modulation formats with digital signal processing (DSP) enabled coherent receivers [6]–[9] that allowed to scale single channel capacity, trading off spectral efficiency with sensitivity requirements. Due to this trade-off, spectral efficiency enabled capacity scaling will not be enough to sustain current capacity growth trends [10]. To overcome this problem, several alternatives have been considered, including spatial division multiplexing (SDM) [10], [11] and multi-band transmission systems [12], [13]. Both approaches exploit the linear gain in capacity that can be obtained by scaling either the number of spatial modes (SDM approach) or the bandwidth used for transmission, as opposed to targeting logarithmic gain in capacity obtained by scaling the signal-to-noise ratio (SNR) of the received signal. The latter can be usually done by means of system redesign (e.g. using better fibers) or by adopting power hungry nonlinear compensation strategies.

Google is currently pursuing both strategies that yield linear gain in capacity. The simplest form of SDM, i.e. the deployment of parallel single mode fibers, is currently adopted in submarine cables [14], while multi-band (C+L) open line systems [4], [15] are globally deployed in the terrestrial long-haul network. In this paper we focus on the latter strategy describing the motivations for C+L system deployment and the business and technical challenges associated with it (Section II–III) in the context of long-haul terrestrial systems. Section IV presents an overview of the optical design aspects to be taken into account when designing C+L systems, and Section V presents a comparison between spatial and bandwidth scaling. Finally, comments and conclusions are drawn in Section VI. The paper will mainly focus on C+L systems, leaving the discussion on design, deployment, and management of open line systems in general to future publications.

II. Motivations for C+L Systems Deployment

Optical communication systems flourished around the C-band spectrum due to the availability of a convenient amplification medium (the Erbium doped fiber [16]) and the low loss value around 1550 nm of standard single mode fiber (SSMF, ITU-T-G.652). In the late 1990's, L-band started being considered as a viable solution to further scale link capacity with relatively low engineering effort compared to C-band only systems [17], [18]. However, the burst of the dot-com bubble halted such developments and it took more than a decade for L-band to become relevant again.

Over the last decade, the so-called open line systems (OLS) have represented a cost-effective way to cope with exponential data traffic growth in a cost-effective manner [15]. In OLS, line systems (amplifiers, optical nodes, etc.) and terminal optics (transponders) are decoupled, enabling lower total cost of ownership (TCO) by mixing and matching line system and transponder vendors and leveraging the faster update cycles of transponders. These cycles are mainly driven by CMOS technology scaling, thus they generally outpace those of common

Manuscript received June 21, 2019; revised October 1, 2019; accepted November 21, 2019. Date of publication December 12, 2019; date of current version March 11, 2020. *(Corresponding author: Mattia Cantono.)*

The authors are with Google LLC, Mountain View, CA 94043 USA (e-mail: mcantono@google.com; rschmogrow@google.com; mnewland@google.com; vijayvusiri@google.com; tad@google.com).

Color versions of one or more of the figures in this article are available online at http://ieeexplore.ieee.org.

Digital Object Identifier 10.1109/JLT.2019.2959272

optical devices such as amplifiers and re-configurable optical add/drop multiplexers (ROADMs). Using the same line system with multiple generations of terminals allows a more efficient equipment utilization and lower TCO. Google has been following an OLS approach since 2010 [4], starting with an arrayed waveguide grating (AWG) based line system operating over the C-band. This initial OLS has then been upgraded to a colorless, directionless, and contentionless (CDC) system, which in its most recent iteration, operates over the C and L bands with a total bandwidth close to 10 THz.

The motivations to deploy C+L systems are manifold. One of the main reasons for which multi-band systems are appealing is associated to the better utilization of fiber resources, as capacity can be scaled without the need for deploying or acquiring new fiber even in low SNR scenarios. Depending on the considered network segment and the scale of the network, this aspect might be critical. Based on our experience, long-haul segments are affected by fiber scarcity, and pulling new fiber even through existing ducts still represents a major cost factor [19]. This represents a smaller issue for metro networks where fiber is in general not scarce, and typical reach is such that high spectral efficiency can be achieved, hence well matching capacity demands. One may argue that deploying two subsequent C band line systems are an advantage with respect to incremental growth. However, some C+L line systems offer an upgrade path from a C only system to a C+L system. As a potential caveat the upgrade may affect existing traffic in the C band since they rely on the same transport fiber. However, this can be mitigated or even eliminated if amplified spontaneous emission (ASE) noise loading is deployed keeping the system stable.

In addition to this, even for long-haul routes with no fiber deficiency, turning up C+L line systems has still some advantages compared to deploying and turning up two independent C-only line systems over two parallel and physically separate fiber rails. We will refer to this simplest form of SDM as 2xC systems. Such a solution is less efficient from a deployment perspective than C+L as it requires to install and configure two independent systems. Furthermore, C+L systems' footprint in terms of space and power is smaller than two C-only systems (2xC). Even though more optical components such as splitters and couplers are required to split/combine C and L band channels, a good level of integration between C and L band components can be achieved at the chassis level, and several system functions (e.g. controllers, monitoring, etc.) can be consolidated into a single platform. Consolidation however can represent a problem in terms of risk of failure of line system components: On the one hand, with a single C+L OLS twice as many channels are exposed to the risk of failure of a single chassis (e.g. an in-line amplifier) compared to the case of two independent C-band OLS. On the other hand, the majority of optical outages that take place in large scale networks are associated with fiber level failures [20], [21], to which both C+L and 2xC solutions are equally exposed. Therefore, for both solutions, network availability considerations need to be pivotal during the overall network design phase [20].

Although system benefits are clear, several challenges are associated to C+L systems both from a technical point of view, and from a business and ecosystem maturity one. Over the last few years several line system vendors started offering C+L open line systems [22]–[24] as a solution to double capacity over existing fiber routes. These efforts pushed forward C+L line system maturity in terms of architectural design and operational management. Despite this, L-band optical components still come at a price premium and can lag in market availability compared their C-band counterparts, even though the bill of material (BOM) is very similar in some cases. This is mostly due to the relatively low volumes of L-band components and the specific design variations that are required in some L-band sub-components such as lasers for transponders and amplifiers to achieve comparable performance to their C-band counterparts. As more and more C+L line systems are deployed, L-band component volumes increase and such premium is likely to be reduced.

In the next section we will focus on the optical challenges associated with C+L band systems.

III. Optical Challenges of C+L Systems

Although the TCO benefits for multi-band communications are evident, several optical challenges need to be considered when designing and operating them. Such challenges are related to propagation impairments, frequency dependent optical fibers characteristics, optical component limitations, and the interplay between all of them.

A. Fiber Propagation Impairments

In addition to the well known linear (loss, chromatic and polarization mode dispersion) and nonlinear effects (Kerr) that represent the main sources of propagation impairments in optical communications, going beyond the C-band utilization triggers wide-band propagation effects that can compromise potential capacity gains. The most relevant one is represented by stimulated Raman scattering (SRS) [25], [26]. Raman Scattering is a nonlinear effect associated with the inelastic scattering of the optical signal traveling in a fiber by silica vibrational modes in the form of optical phonons. Such scattering process is significant over spectral occupations of the order of few THz. Its first order effect on wavelength division multiplexed (WDM) optical signals is an energy transfer from higher frequency channels to lower frequency ones hence producing a tilt in the observed power spectrum of the WDM comb [27]. As SRS efficiency in silica core fiber is maximum for signals with a frequency separation of approximately 13 THz [26], it is relevant for multi-band systems, including C+L ones. During propagation, L-band carriers are pumped by the ones occupying the C-band causing a significant tilt in the power spectrum of the signal. Such energy transfer is critical throughout all of the system life, as signal add/drop, if not properly managed, can cause severe penalties to existing channels. In addition, it has been shown that SRS interacts with the Kerr effect [28]–[31], contributing to a frequency dependent generation of nonlinear interference (NLI) noise. In order to correctly model both SRS and NLI generation over wide-band systems, all fiber parameters with a frequency dependence need to be taken into account, in particular loss,

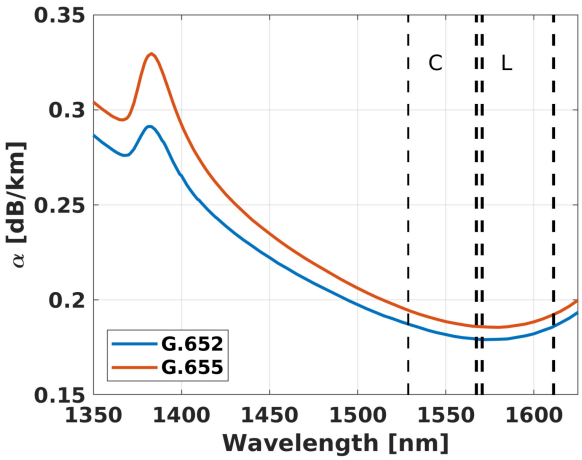

Fig. 1. Typical loss profiles of G.652 and G.655 fibers.

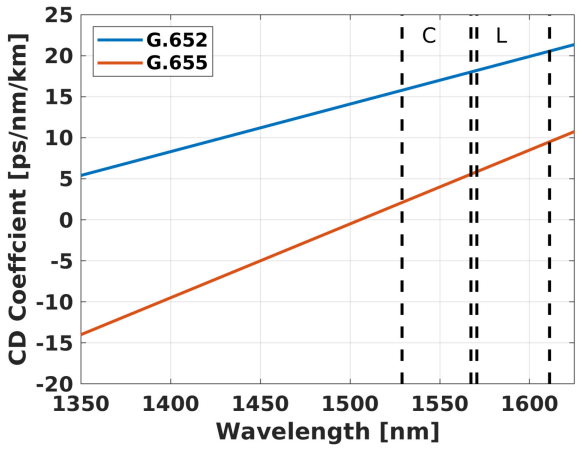

Fig. 2. Typical chromatic dispersion coefficient of G.652 and G.655 fibers.

dispersion, and nonlinear coefficients. Fig. 1 shows the typical attenuation per km as a function of wavelength for two of the most widely deployed single mode fiber types, namely G.652 and G.655 [32], [33]. It can be seen that the low loss region of wavelengths significantly extends beyond the C-band providing the opportunity to place optical signals outside of it. The chromatic dispersion (CD) coefficient for the same two example fiber types is depicted in Fig. 2. We can see that chromatic dispersion for these widely deployed fiber types tends to be larger in the L-band. Not only can the larger CD value be handled by state-of-the-art coherent transponders but NLI noise may even be lower due to decreased phase matching conditions [34]. Extending the transmission window towards larger wavelengths appears to be the natural choice since efficient amplification schemes are available as described in the following section.

B. *Optical Amplification*

Several options exist to achieve optical amplification over C and L bands (Fig. 3). The most widely used and deployed options today rely on a single erbium doped fiber amplifier (EDFA) for each optical band and an associated demuxing/muxing architecture (Fig. 3(a)). EDFAs represent a mature technology also for L-band amplification as it leverages more than 20 years of research and engineering experience [35]. Compared to the C-band EDFA, the L-band EDFA presents some performance penalties inherently caused by the amplification mechanism itself. In particular, L-band signal amplification utilizes the long wavelength tail of the Erbium gain spectrum and in this region Erbium absorption and emission coefficients are much smaller than in the C-band [35]. This in tendency yields lower gain than C-band amplifiers, usually compensated for by longer EDF coils. As a consequence it causes a degradation in power conversion efficiency and noise figure penalty due to the build up of backward propagating ASE noise. Alternative approaches based on different doping materials have been considered, e.g. tellurite [36] or bismuth [37], but proper pump optimization schemes have been found instead, e.g. pump engineering or secondary pumping [38], [39] to limit noise and gain penalties of L-band EDFAs, which today are below 1 dB for commercially available modules. An additional capacity penalty associated to this architecture is related to the bandwidth waste caused by the guard-band between C and L band of the demuxing/muxing structure before and after the EDFAs. This guard-band is typically around 400 GHz. In addition to this, a noise figure penalty due to the non zero insertion loss of the muxing architecture is present. Amplifier designs to remove such guard-band (Fig. 3(b)) have been proposed in the past at the expense of a more complicated design with multiple amplification stages and gain equalization per band [18]. More recently, similar single wide-band amplifiers have been proposed using semiconductor optical amplifier (SOA) [40]. However they still have to be adopted in commercially available systems due to concerns associated with SOA nonlinearities such as cross gain modulation and increased noise figure. Despite the fact that separate C and L band amplifiers slightly lower overall available transmission bandwidth, it simplifies operations as it allows to turn up bands independently as capacity grows.

Similarly to what is done in C-band only systems, EDFA based amplification is usually supplemented by backward propagating Raman amplification (Fig. 3(c)), in form of a typical hybrid Raman-EDFA amplifier configuration [41]. Hybrid amplification schemes are widely adopted as Raman amplifiers allow to increase system SNR thanks to an improved noise figure. Therefore Google currently deploys them in the almost every long haul route. In modern hybrid Raman/EDFA amplifiers, equivalent noise figure values lower than -1 dB can be achieved [41]–[43]. Raman amplifiers rely on the nonlinear power transfer enabled by SRS between one or more strong pumps and the WDM signal. The spectral separation between pumps and signal is adjusted in order to optimize the gain profile and minimize noise figure variations. To achieve gain flatness <1 dB over the C and L band, Raman amplifiers with more than 5 pumps have been proposed [44]. Although the positive system impact of Raman amplifiers is clear and well accepted, a few aspects must be taken into account in the context of C+L and multi-band systems. One of the main aspects is the inherent strong noise figure dependency of Raman amplifiers, especially for wide-band

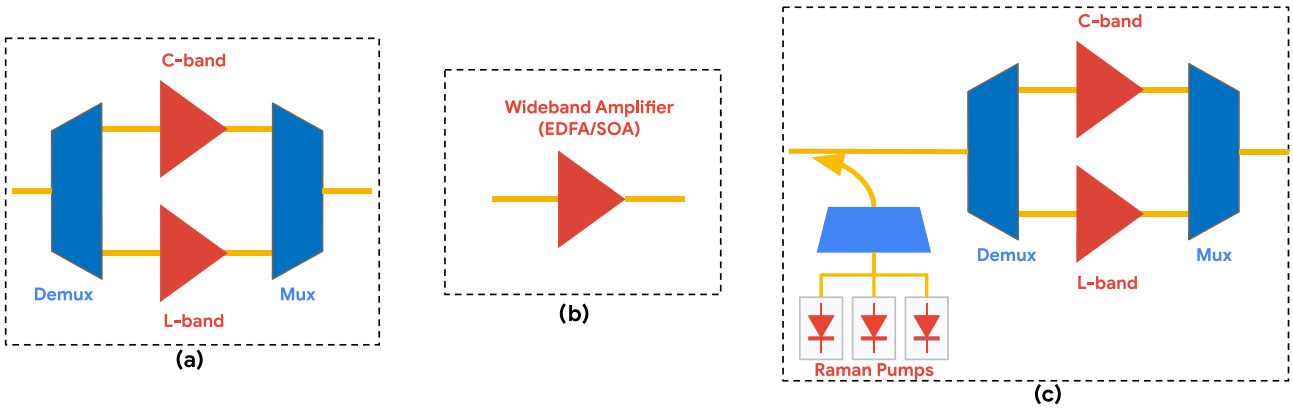

Fig. 3. Amplification options for C+L systems. (a) C and L EDFAs with mux/demux, (b) single wide-band amplifier (EDFA/SOA), and (c) Hybrid EDFA/Raman with multi-pump Raman amplifiers.

amplification. Such behavior arises from many factors [45], [46]. First, the amount of ASE noise generated by a Raman amplifier depends on the spectral distance between the signal and the pumps: The closer the two, the stronger the ASE. This implies that short wavelength channels experience a higher noise figure compared to the long wavelength ones. In addition to this, SRS between short and long wavelength signals of the WDM comb constitutes an additional loss mechanism for short wavelength signals. Such gain imbalance across the comb contributes to and causes a higher noise figure at short wavelengths compared to long ones. The net effect of this imbalance is that, even if power variations across the WDM comb at the output of the fiber are small, large SNR variations might occur. Co-propagating Raman pumps help mitigate this issue. However they cause an overall nonlinear SNR penalty due to high power at the beginning of the fiber span [43] and an increased relative intensity noise (RIN) transfer between pumps and signals [45]. Additional considerations need to be taken to understand other potential limiting factors due to pump-pump and pump-signal interactions [47]. One of the most potentially detrimental ones is represented by pump-pump and pump-signal four-wave mixing (FWM) [48], [49]. Spurious FWM tones can be generated within the WDM signal comb, causing large performance penalties at some wavelengths. This is especially true for low dispersion fibers where the Raman pumps are centered close to the zero dispersion wavelength of the fiber in which case the FWM efficiency is maximized. Thankfully, such effect can be mitigated by properly optimizing the pumps power profile and wavelengths.

All these being considered, a correct modeling of Raman amplification, including both gain and noise figure characteristics, is fundamental when designing and correctly operating multi-band transmission systems. Fortunately, this challenge has already been successfully solved by multiple network equipment manufacturers (NEM) who offer both C+L line system and transponder solutions for some time. More detailed aspects of C+L system deployment and operation follow in Section III-D.

C. Transponders

Designers and operators of C+L optical networks should be aware of all performance impacting, frequency dependent behaviors of optical components. These include for example frequency dependent responses of deployed transponders that might lead to non-uniform bit-error ratio (BER) performance across the WDM spectrum. Among these effects it is worth mentioning the different received power sensitivity of C and L band transponders, as well as the potentially lower output power of L-band transponders due to the aforementioned limitations of L-band EDFAs. We want to emphasize that, in Google's experience, the described challenges are far from being substantial. However, it is worth considering them when troubleshooting sporadic optical routes exhibiting unexpected behaviour.

D. Operational Aspects

In the following section we elaborate on some of the operational implications we have observed that are associated with multi-band optical communication links such as adding and dropping wavelengths (intentionally and unintentionally) as well as the impact of the fiber plant itself (installation, splicing, connectors, etc.).

In general, at the time of deployment only a subset of the available bandwidth is used to accommodate optical signals. Usually there is a requirement that adding or removing optical signals from the line must not impact any of the other static channels while doing so. One may argue that this is even more critical and challenging since a C+L system accommodates twice the amount of optical signals with respect to its C band counterpart. Therefore the odds for new signal additions as well as the probability for transponder failures (since there are more transponders) and amplifier or node failures increases as well. A way to mitigate if not eliminate a large portion of potential impact on existing signals is ASE noise loading. Unused spectrum is filled with ASE such that potential end of life conditions are present on day one. New signals can now be added gradually without creating significant transients in the system. Similarly in case of failure, e.g. loss of signal in parts of the spectrum, ASE can be dynamically injected to restore the system dynamics. The only down-side of this approach is that reduced nonlinear noise in scarcely loaded links cannot be leveraged for larger capacity initially. However, doing so at our scale would result

in unacceptable operational complexity every time new carriers are being added or removed.

The next aspect we want to address are failures of an entire band as e.g. observed if one of the two EDFA amplifiers fails or a fiber connector is accidentally disconnected. We can distinguish between two scenarios, namely with and without ASE noise loading. For systems without ASE noise loading we decided to treat any band failure as a failure of the whole system, i.e. equivalent to a fiber failure. As a consequence, potential device failures increase the probability that traffic is lost on a C+L band system over its C-band only counterpart. In practice however we observe fiber related failures dominate over device failures. For ASE loaded systems, noise can be injected to mitigate the effect of a band failure. However, while the downtime may be significantly shorter, there may still be an impact on existing carriers in the other band. In general, changes in underlying failures in time (FIT) rates should be addressed at the stage of network design and is often a multi-layer consideration.

Finally, we would like to discuss multi-band related aspects with respect to the fiber plant itself, e.g. bending of the fiber, as both micro-bends and macro-bends lead to frequency dependent loss. Both are undesirable effects that are either introduced during manufacturing (micro-bends) or caused by the fiber installation itself (macro-bends). In general the added attenuation affects signals with different mode field diameters (MFD) differently. Even though all signals propagate as the same mode in single mode fiber, their respective confinement in the fiber core is a function of frequency or wavelength. It has been discovered that shorter wavelength (C-band) have a smaller MFD than longer wavelength (L-band) and are hence less affected by either micro or macro-bends [50], [51].

In order to assess the potential impact of fiber bends on C+L system deployments we evaluated multiple fiber routes in Google's long-haul network with respect to bends, splice, and connector losses. To this end the fiber plant has been characterized with optical time domain reflectometry (OTDR) at 1550 nm (C-band) and 1625 nm (L-band) wavelengths. The target was to assess the potential impact of C+L deployment with respect to fiber remediation efforts (re-splicing, connector cleaning, macro-bend removal, etc.). We consider all splices, connectors, and bends that exceed a loss delta between C and L-band of 0.08 dB (corrected for the intrinsic fiber loss profile). We further broke down the results between fiber routes in North America and Europe. The obtained probability mass functions (PMF) for connector and splice loss difference (loss at 1550 nm–loss at 1625 nm) distributions are depicted in Fig. 4. The total number of events recorded was $>\sim 1300$ with more splices than connectors. It can be concluded that the mean of the loss difference is close to 0 dB while connectors tend to present a larger standard deviation than splices and bends. In addition, approximately 95% of all instances that may require remediation effort satisfied the <0.08 dB threshold. Hence, while there were some instances where the use of L-band warranted some additional remediation efforts, the vast majority did not. Thus we concluded that using C+L systems rather than C-band only systems does not create a significant additional burden on the fiber plant remediation. Notice that the spectral separation of the two selected wavelengths is large enough to detect macro-bend loss induced loss variations in the fiber (see Fig. 4 in [51], Fig. 6 in [52]).

IV. Design of C+L Optical Networks

In order to properly design and operate OLS based transport networks at scale, reliable prediction of expected optical performance is fundamental. In dispersion uncompensated transmission scenarios, it has been widely shown that fiber propagation impairments caused by the interplay of loss, chromatic dispersion, and Kerr nonlinearity can be well approximated as an additive Gaussian noise on any single frequency, named nonlinear interference (NLI) [53], [54], also in presence of SRS [29], [55]. As all major propagation impairments, i.e. amplified spontaneous emission (ASE) noise, and NLI can be modeled as Gaussian disturbances, a unique metric in the form of a signal-to-noise ratio (SNR) can be used to assess the performance of each channel. This metric has been defined as effective or generalized SNR (GSNR) and is the ratio between the power of the useful signal divided by the sum of the powers of all noise sources - such as ASE and NLI–evaluated in the signal bandwidth, centered at wavelength λ_i

$$\mathrm{GSNR}(\lambda_i) = \left[\frac{1}{\mathrm{SNR}_{\mathrm{LIN}}(\lambda_i)} + \frac{1}{\mathrm{SNR}_{\mathrm{NLI}}(\lambda_i)}\right]^{-1} \quad (1)$$

Note that any propagation impairment that can be modeled as Gaussian noise can be properly included in the definition of GSNR. All noise sources not associated to the line side of an optical system (e.g. transponders electrical noise, implementations and other non ideal characteristics) are not included in the definition of GSNR. GSNR can be directly tied to the achievable system capacity either using the Shannon formula, or by referring to specific transponders characteristics.

Modeling tools used during the network design phase should correctly model GSNR, meaning that they should be able to provide a precise estimation of both linear (ASE from amplifiers) and nonlinear noise. It should be noted that GSNR is typically optimized when the linear (ASE) noise is twice as large as NLI noise [56]. In such operating condition, propagation impairments are mainly linear in nature. Therefore the accuracy of GSNR estimations in this regime largely depends on the accurate characterization of linear noise sources, thus a precise characterization of the photonic components (EDFAs, Raman cards, DGEs, ROADMs) responsible for ASE build up in the system is pivotal. Furthermore, given the optical challenges highlighted in Section III, all GSNR estimations need to be performed taking into account all frequency dependencies when dealing with C+L systems, with focus on SRS, and noise/gain dependencies vs frequency.

V. System Analyses

A. Methodology

Most optical vendors provide tools for designing and predicting an optical communication link. In addition even open source initiatives started tackling the problem [57]. Within Google, an

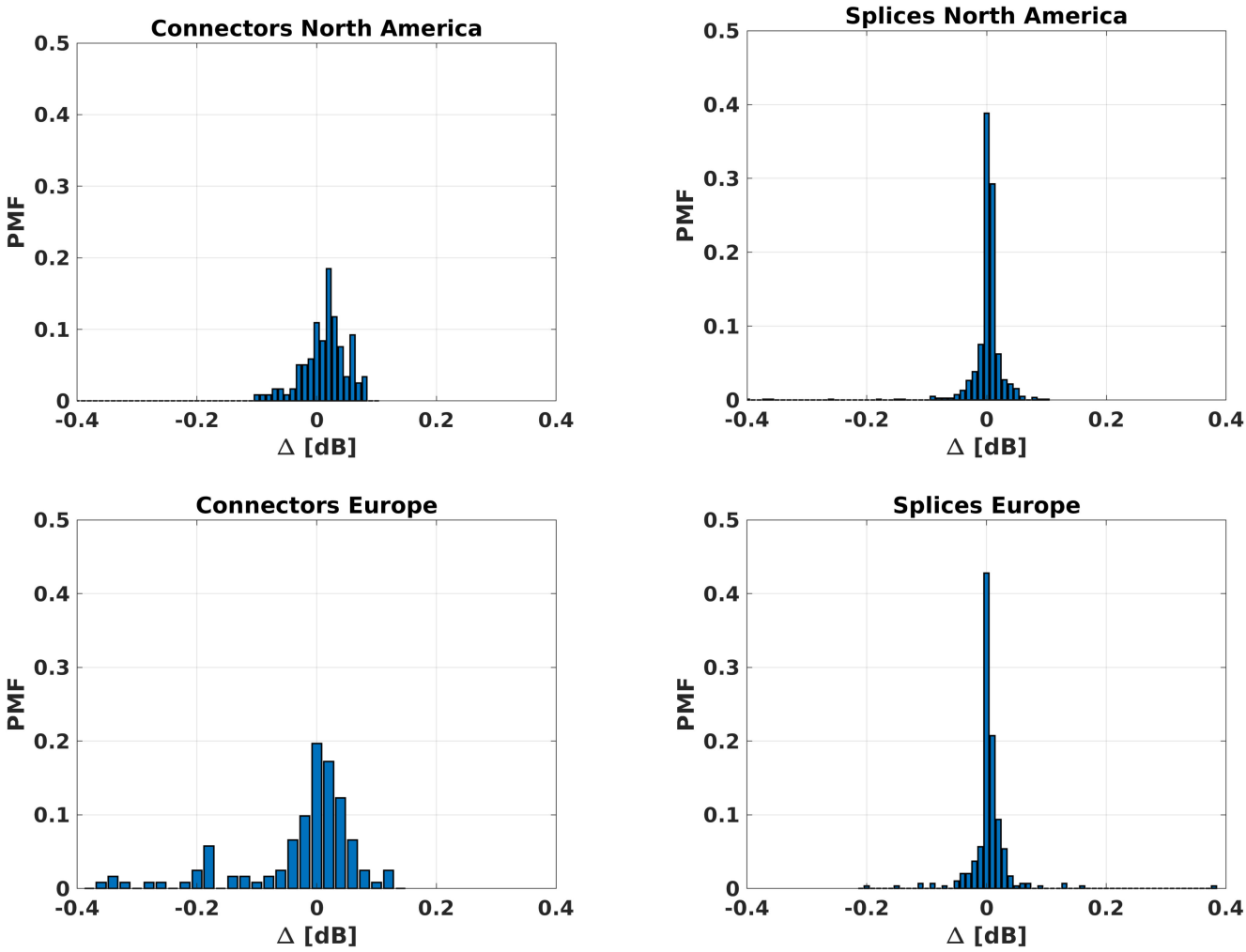

Fig. 4. Probability density mass functions for loss difference (loss at 1550 nm–loss at 1625 nm) for connectors and splices or bends in North America and Europe.

internal optical design tool has been developed over the years. We obtained detailed characteristics and data on all line system components such as amplifiers and fibers from our suppliers. With this rich data set we are able to model the line system behavior. Limitations arise from the fact that we have to rely on typical values for characteristics such as gain, attenuation, or noise figure data. For estimating the nonlinear noise contributions we leverage the standard split step Fourier method [58]. We chose the step size such that a further reduction virtually did not change the outcome of the nonlinear simulation. Similarly, we carefully selected random patterns for signal generation to minimize dependencies on the pattern itself and the length thereof thus trading off absolute accuracy and computational speed. Additionally, all signals were pre-dispersed such that patterning due to the modulation format is mitigated. Therefore, nonlinear results presented in the subsequent sections may show slight variations caused by the random patterns used. The contribution of these variations to the overall accuracy is negligible compared to e.g. using typical device and fiber data rather than thoroughly characterizing each element in the field which is operationally prohibitive. Finally please note that while we operate different transponder platforms on various optical grids, the simulations performed in this paper used 32 GBd signals and a 50 GHz frequency spacing. While the results can be extended to other grids (e.g. 75 GHz, 100 GHz, or even mixed) an analysis of flex-grid and symbol rate impact is beyond the scope of this paper.

In order to obtain a fair comparison between C and C+L simulations, we individually optimize the power spectral density (PSD) into each fiber span. In general we adopt a very simple local optimization on a per-channel basis, meaning we compute the power variations required for each channel and average them across C and L bands. As a result, we obtain a single power level adjustment for both bands. Such type of optimization is feasible as not all amplifiers have dynamic gain equalizer (DGE) capabilities. Hence power settings can only be realized considering a uniform per-channel power. For DGEs we apply a similar strategy for the sake of simplicity. Note that the same optimization strategy is applied for both C-only and C+L designs. Please note that more advanced optimization strategies exist [59], [60], however discussing them is beyond the scope of this paper.

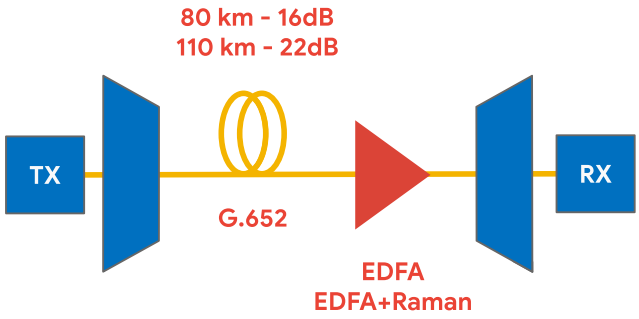

Fig. 5. Simulation setup for single span analyses.

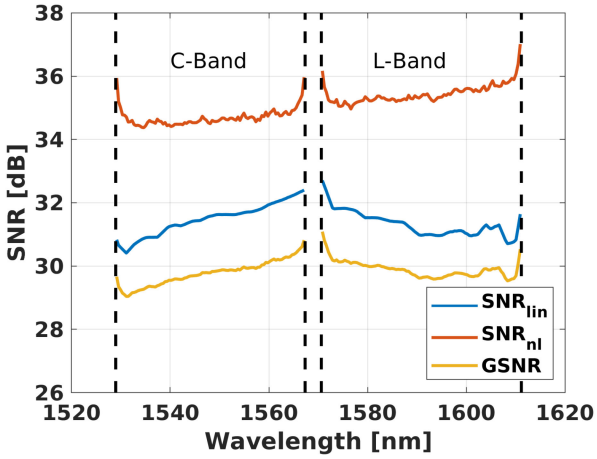

Fig. 6. Single span, G.652, 80 km, 16 dB loss without Raman amplification.

The system results presented in the next sections were obtained with Google's internal design tool, which has been extensively validated over the years with field measurements showing consistent GSNR estimations within 0.5 dB. Please note that discussed results are for a specific line system with its technical limitations so that absolute values in terms of optimum power or GSNR may differ for other systems. Nonetheless we believe that relative results, i.e. C vs. C+L performance can be observed using different types of line systems including generic ones. We will show that, depending on the fiber characteristics, C+L systems have the potential to more than double the capacity of the investigated optical routes.

B. Single Span Analyses

In order to illustrate the expected SNR performance of a C+L system we look at two scenarios each utilizing G.652 and an EDFA based C+L node. For both example single span systems, as depicted in Fig. 5, we plot the linear SNR (caused by ASE noise), the nonlinear SNR (caused by NLI), and the GSNR (see Section IV) as a function of wavelength. We select a flat launch power per channel per band for a fully loaded line and optimize for maximum GSNR.

The results of the first 80 km and 16 dB span simulation are depicted in Fig. 6. For the nonlinear noise contribution described by SNR_{NLI}, it can be seen that there is a tilt with more NLI in the C-band. This can be attributed to the larger chromatic dispersion coefficient in the L-band and hence reduced phase matching. While this dispersion slope effect is already visible for ITU-T-G.652 it is even more pronounced when using fiber with lower C-band dispersion such as ITU-T-G.655. It can be concluded that NLI in the L-band tends to be lower leading to better nonlinear performance. Next we analyze the linear noise contribution or SNR_{LIN}. L-band EDFAs tend to have a larger noise figure than their C-band counterparts. However, due to SRS induced energy transfer between C-band carriers and L-band carriers the resulting SNR_{LIN} is comparable between C and L-band in this example ranging from 28 dB–30 dB. Finally, the GSNR shows similar performance between C and L-band carriers with only the low wavelength half of the C-band experiencing slightly degraded performance.

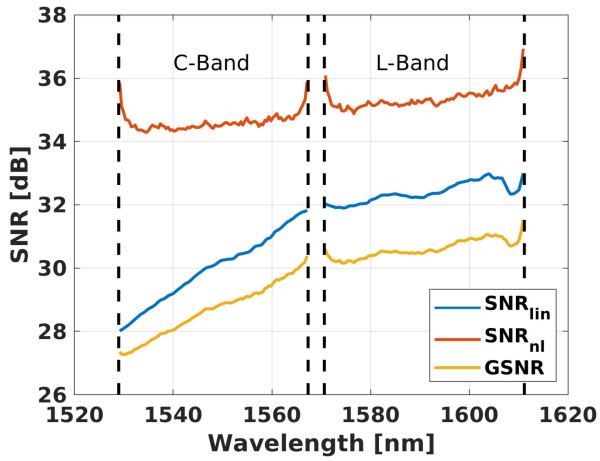

Fig. 7. Single span G.652 with Raman amplification: 110 km, 22 dB loss.

Next we analyze a single span system terminated by a Raman and EDFA hybrid node. Again we optimize the launch power per band to maximize GSNR but keep the per carrier power in each band constant. The results of this 110 km and 22 dB average loss simulation is shown in Fig. 7. Please note that compared to the previous example (Fig. 6), the span is 30 km longer, there is Raman gain, and the launch power is different. In sum these effects by chance lead to a similar nonlinear noise contribution. The linear part SNR_{LIN} however is very much different, which is ultimately reflected in the GSNR. Here we observe a much more pronounced tilt in the C-band which is caused by the noise figure characteristics of the Raman amplifier (see Section III-B). L-band performance is enhanced but comes at the price of degraded C-band performance. Therefore it is essential to consider both the impact of enhanced L-band and degraded C-band performance when comparing the achievable capacity. One way to mitigate the GSNR delta is to treat C and L bands separately when configuring transponder modes (e.g. 8QAM). To elaborate more, we consider a test link and discuss the results and strategies in detail in Section V-C.

C. Test Link Analysis

In order to compare a traditional extended C-band system with 4.8 THz total bandwidth and a C+L system with 9.6 THz

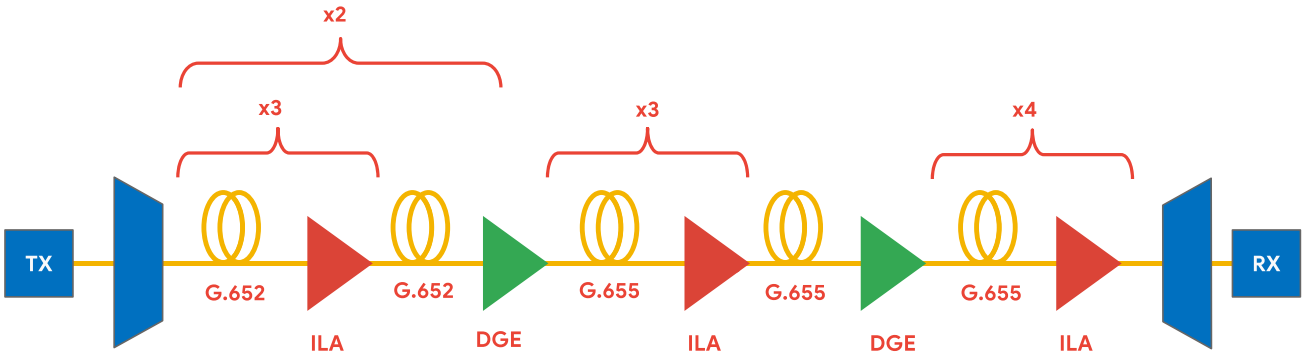

Fig. 8. Simulation setup: 8 G.652 + 8 G.655 spans. Dynamic gain equalization for spectrum flattening is performed every fourth span. In-line amplifier type is picked to optimize performance.

bandwidth we create a test link comprising a total of 16 spans, see Fig. 8. The test link consists of the two previously described fiber types, namely ITU-T-G.652 and ITU-T-G.655. Furthermore we chose half of the spans to be amplified by EDFAs only with 80 km length and 16 dB loss and the other half utilizing Raman EDFA hybrid nodes with 110 km span length and 22 dB loss. To correct for power ripple build up we place a DGE after each fourth span as is common practice. Again the simulation is conducted with a fully loaded line.

Since the goal is to obtain a fair comparison between the C and the C+L system simulation, launch powers are individually optimized to maximize GSNR. For the C-band only simulation we use the same model for C-band EDFAs as is used in the C+L simulation. It should be noted that typical line amplifiers may comprise filters to drop the optical supervisory channel (OSC) as well as another filter to enable OTDR measurements. The insertion loss of these filters is assumed to be 0.5 dB each. If we further assume that the C/L splitter adds an additional 0.5 dB of insertion loss to each band, we can rearrange the optical elements to result in no additional loss for the C+L band amplifier over its C-band only counterpart. This is achieved by placing the OSC and OTDR filters in separate paths. Finally, the model for the Raman amplifier is adjusted to reflect an optimized design for each of the scenarios (C and C+L) with 5 Raman pumps in both cases.

The SNR results for the described test link are illustrated in 9. Again we plot the linear, nonlinear, and combined noise contribution of the optical link for both the C-band only case (dashed lines) and the C+L band system (solid lines). It can be seen that the C-Band performance of the C-only system exceeds its C+L band counterpart. This is mostly due to energy transfer from C-band carriers to L-band carriers effectively increasing the C-band loss. As a side effect the nonlinear performance of the C+L band C carriers is slightly better. In summary there is a worst case delta between C and C+L GSNR of 0.5 dB. Even though the C-band of the C+L system is slightly penalized, the L-band GSNR is higher throughout.

Next we analyze the achievable capacity comparing two C-band only systems and a C+L system. We consider different variations to the well-known Shannon capacity formula [61] to include transponders internal noise penalties, coding gap and rate quantization [62]. The capacity for a signal of bandwidth B

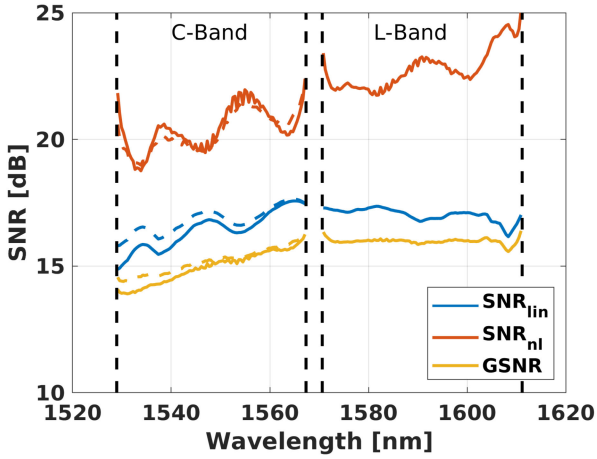

Fig. 9. C (dashed lines) and C+L (solid lines) 1080 km link simulation results.

is then given by

$$C = R_c \left\lfloor \frac{1}{R_c} \left[2B \log_2 \left(1 + \frac{\text{SNR}}{\Gamma} \right) \right] \right\rfloor \tag{2}$$

where R_c represents the client rate, Γ is the coding gap, and SNR is given by

$$\text{SNR} = \left[\frac{1}{\text{GSNR}} + \frac{1}{\text{SNR}_{\text{TRX}}} \right]^{-1} \tag{3}$$

where SNR_{TRX} is the SNR associated with the internal noise of the transponder, i.e. of the transmitter and receiver, and GSNR is the GSNR of the signal at the considered wavelength. All SNR values are in linear units.

Using the GSNR values of Fig. 9, we compute the achievable capacity under different assumptions. We first compute the Shannon capacity, removing rate quantization while setting $\Gamma = 1$ and SNR = GSNR in Eq. 2. Then we consider non quantized transponders with a 3 dB coding gap and a 22 dB SNR_{TRX}. Finally we quantize the obtained rate assuming $R_c = 25$ Gbps, $R_c = 50$ Gbps, $R_c = 100$ Gbps. Results are reported in Table I. In all cases, the achievable capacity of the C+L configuration is greater than or equal to that of the 2xC with a maximum improvement of 4.4% (44.7 Tbps vs. 42.8 Tbps) for the Shannon transponder with penalties and 50 G quantization. By removing

TABLE I
ACHIEVABLE CAPACITY IN 2XC AND C+L FOR THE 1080 KM SIMULATED LINK OF FIG. 8

	Shannon Capacity	Shannon Capacity w/ Penalty	Shannon Capacity w/ Penalty 25G Client	Shannon Capacity w/ Penalty 50G Client	Shannon Capacity w/ Penalty 100G Client
2xC [Tbps]	62.50	47.61	45.40	42.80	38.40
C+L [Tbps]	63.60	48.47	46.35	44.70	38.40
$\Delta_{C+L/2xC}$ [%]	1.8%	1.8%	2.1%	4.4%	0%

quantization, the capacity improvement shrinks to 1.8% both with and without extra penalties. With an aggressive 25 Gbps quantization, the C+L configuration can accommodate for an extra 2.1% of capacity (46.35 Tbps vs. 45.40 Tbps). Assuming 100 G quantization, the two configurations yield the same total capacity. It should be noted that these results have been obtained assuming a nonuniform rate assignment across the spectrum, or in other words, locally maximizing achievable capacity at each wavelength. This allows to leverage the higher GSNR of the L-band to harvest more system capacity. The operational complexity increase of non-uniformly applying configurations across transponders can be easily mitigated adopting automation practices during deployment [63]. It is worth mentioning that for the simulated link of Fig. 8, when considering quantized transponders, uniformly applying rates over the spectrum based on the GSNR of the worst performing wavelength does not cause any capacity penalty between C+L and 2xC configurations, even though the minimum GSNR in the C+L configuration is 0.5 dB worst than the C-only one. When looking at the performance of each band one may conclude that a parallel L-band only system has the potential to outperform both C+L and 2xC solutions. While the increased dispersion in the L-band is generally beneficial, the noise figure of L-band EDFA tends to be higher, and a major boost to L-band performance in C+L systems originates from SRS induced energy transfer between C and L-band carriers. The latter effect will not be present in L-band only systems.

D. Production Network C+L Link

After comparing C and C+L band performance in a very controlled simulation environment we want to now look at performance observed in the field and compare it to the predicted performance obtained by our simulation tool. To this end we gather data from a 3177 km fiber link that is part of our production network. The aggregate loading of C and L bands is 98 % with all optical signals carrying production traffic of ≈19 Tbit/s. We derived GSNR from pre-forward error correcting (FEC) Q values read from the transponders using typical back to back Q vs. SNR curves. The results can be seen in Fig. 10. The open circles are measurements and the two dashed lines represent the upper and lower bound of the prediction obtained with the simulation. Deviations may stem from the fact that we use typical values for both line system components such as amplifiers and for transponders in our simulation. Nevertheless it can be concluded that the simulation agrees with the field data within the tolerance limits. These results also show an almost fully loaded C+L communication link carrying production traffic.

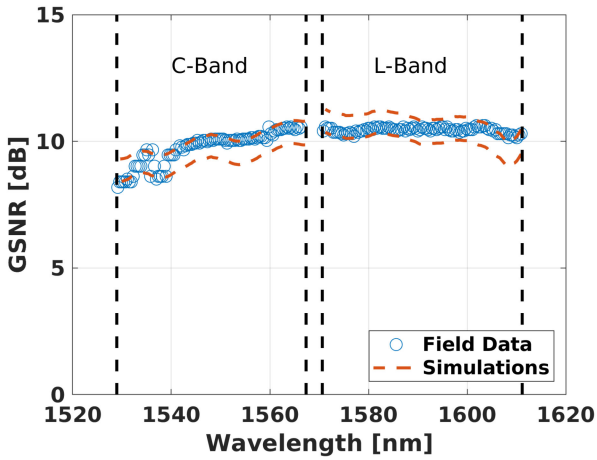

Fig. 10. Results for 3177 km production network link with 98% loading.

VI. CONCLUSIONS

In this paper we have presented opportunities and challenges of C+L transmission systems, showing how they represent a viable solution to scale capacity in terrestrial networks. Leveraging Google's experience in designing, deploying and operating a global C+L backbone network, we have reviewed business, operational and technical challenges of C+L band transmission systems demonstrating how they represent a technologically mature and economically viable alternative to parallel C-band systems. Through simulation results we have shown how C+L systems do not exhibit capacity penalties compared to parallel C-band systems, but can even unlock moderate capacity gains ($<5\%$) when deployed on low dispersion fiber routes thanks to the better propagation performance of the L-band.

ACKNOWLEDGMENT

The authors would like to thank Joe Lutz and Yekaterina Arestova for fruitful discussions on fiber characterization and comparison in C and L bands. The authors would further like to thank Massimiliano Salsi for his valuable inputs and Corning for providing typical fiber data for G.652 and G.655 types (Fig. 1).

REFERENCES

[1] A. Singh *et al.*, "Jupiter rising: A decade of CLOS topologies and centralized control in Google's datacenter network," *Commun. ACM*, vol. 59, no. 9, pp. 88–97, Aug. 2016. [Online]. Available: http://doi.acm.org/10.1145/2975159

[2] C. F. Lam, H. Liu, B. Koley, X. Zhao, V. Kamalov, and V. Gill, "Fiber optic communication technologies: What's needed for datacenter network operations," *IEEE Commun. Mag.*, vol. 48, no. 7, pp. 32–39, Jul. 2010.

[3] X. Zhao, V. Vusirikala, B. Koley, V. Kamalov, and T. Hofmeister, "The prospect of inter-data-center optical networks," *IEEE Commun. Mag.*, vol. 51, no. 9, pp. 32–38, Sep. 2013.

[4] V. Kamalov *et al.*, "Lessons learned from open line system deployments," in *Proc. Opt. Fiber Commun. Conf. Exhib.*, Mar. 2017, Paper M2E.2.

[5] P. J. Winzer, D. T. Neilson, and A. R. Chraplyvy, "Fiber-optic transmission and networking: The previous 20 and the next 20 years," *Opt. Exp.*, vol. 26, no. 18, pp. 24190–24239, Sep. 2018. [Online]. Available: http://www.opticsexpress.org/abstract.cfm?URI=oe-26-18-24190

[6] G. Gavioli *et al.*, "100Gb/s WDM NRZ-PM-QPSK long-haul transmission experiment over installed fiber probing non-linear reach with and without DCUs," in *Proc. 35th Eur. Conf. Opt. Commun.*, Sep. 2009, pp. 1–3.

[7] D. S. Ly-Gagnon, S. Tsukamoto, K. Katoh, and K. Kikuchi, "Coherent detection of optical quadrature phase-shift keying signals with carrier phase estimation," *J. Lightw. Technol.*, vol. 24, no. 1, pp. 12–21, Jan. 2006.

[8] V. Curri, P. Poggiolini, A. Carena, and F. Forghieri, "Dispersion compensation and mitigation of nonlinear effects in 111-Gb/s WDM coherent PM-QPSK systems," *IEEE Photon. Technol. Lett.*, vol. 20, no. 17, pp. 1473–1475, Sep. 2008.

[9] D. van den Borne, V. A. J. M. Sleiffer, M. S. Alfiad, S. L. Jansen, and T. Wuth, "POLMUX-QPSK modulation and coherent detection: The challenge of long-haul 100G transmission," in *Proc. 35th Eur. Conf. Opt. Commun.*, Sep. 2009, pp. 1–4.

[10] P. J. Winzer and D. T. Neilson, "From scaling disparities to integrated parallelism: A decathlon for a decade," *J. Lightw. Technol.*, vol. 35, no. 5, pp. 1099–1115, Mar. 2017.

[11] P. J. Winzer, "Energy-efficient optical transport capacity scaling through spatial multiplexing," *IEEE Photon. Technol. Lett.*, vol. 23, no. 13, pp. 851–853, Jul. 2011.

[12] A. Napoli *et al.*, "Towards multiband optical systems," in *Proc. Adv. Photon. (BGPP, IPR, NP, NOMA, Sensors, Netw., SPPCom, SOF)*, 2018, Paper NeTu3E.1. [Online]. Available: http://www.osapublishing.org/abstract.cfm?URI=Networks-2018-NeTu3E.1

[13] J. K. Fischer *et al.*, "Maximizing the capacity of installed optical fiber infrastructure via wideband transmission," in *Proc. 20th Int. Conf. Transparent Opt. Netw.*, Jul. 2018, pp. 1–4.

[14] V. Vusirikala, "A quick hop across the pond: Supercharging the Dunant subsea cable with SDM technology," Apr. 2019. [Online]. Available: http://tiny.cc/blr37y

[15] V. Vusirikala, X. Zhao, T. Hofmeister, V. Kamalov, V. Dangui, and B. Koley, "Scalable and flexible transport networks for inter-datacenter connectivity," in *Proc. Opt. Fiber Commun. Conf. Exhib.*, Mar. 2015, Paper Tu3H.1.

[16] R. J. Mears, L. Reekie, I. M. Jauncey, and D. N. Payne, "Low-noise erbium-doped fibre amplifier operating at 1.54m," *Electron. Lett.*, vol. 23, no. 19, pp. 1026–1028, Sep. 1987.

[17] M. Yamada, H. Ono, T. Kanamori, S. Sudo, and Y. Ohishi, "Broadband and gain-flattened amplifier composed of a 1.55 /spl mu/m-band and a 1.58 /spl mu/m-band Er/sup 3+/-doped fibre amplifier in a parallel configuration," *Electron. Lett.*, vol. 33, no. 8, pp. 710–711, Apr. 1997.

[18] Y. Sun *et al.*, "A gain-flattened ultra wide band EDFA for high capacity WDM optical communications systems," in *Proc. 24th Eur. Conf. Opt. Commun.*, Sep. 1998, vol. 1, pp. 53–54.

[19] G. Wellbrock and T. J. Xia, "How will optical transport deal with future network traffic growth?" in *Proc. Eur. Conf. Opt. Commun.*, Sep. 2014, Paper Th.1.2.1.

[20] R. Govindan, I. Minei, M. Kallahalla, B. Koley, and A. Vahdat, "Evolve or die: High-availability design principles drawn from Googles network infrastructure," in *Proc. ACM SIGCOMM Conf.*, 2016, pp. 58–72. [Online]. Available: http://doi.acm.org/10.1145/2934872.2934891

[21] M. Ghobadi and R. Mahajan, "Optical layer failures in a large backbone," in *Proc. Internet Meas. Conf.*, 2016, pp. 461–467. [Online]. Available: http://doi.acm.org/10.1145/2987443.2987483

[22] S. Hardy, "Nokia upgrades 1830 PSS packet-optical transport family with new coherent chipsets, improved multi-rate performance," 2016. [Online]. Available: http://tiny.cc/fmr37y

[23] J. Gill, "Future-proofing your network with Infinera C+L," 2018. [Online]. Available: https://www.infinera.com/future-proofing-your-network-with-infinera-cl/

[24] K. Jordan, "The benefits of an integrated C&L-band photonic line system," 2019. [Online]. Available: https://www.ciena.com/insights/articles/The-benefits-of-an-integrated-C%L-band-photonic-line-system.html

[25] C. V. Raman, "A new radiation [reproduced from *Indian J. Phys.*, 1928, 2, 387–398]," *Current Sci.*, vol. 74, no. 4, pp. 382–386, 1998. [Online]. Available: http://www.jstor.org/stable/24101519

[26] R. Stolen and E. Ippen, "Raman gain in glass optical waveguides," *Appl. Phys. Lett.*, vol. 22, no. 6, pp. 276–278, 1973.

[27] M. Cantono, V. Curri, A. Mecozzi, and R. Gaudino, "Polarization-related statistics of Raman crosstalk in single-mode optical fibers," *J. Lightw. Technol.*, vol. 34, no. 4, pp. 1191–1205, Feb. 2016.

[28] G. Agrawal, *Nonlinear Fiber Optics* (Electronics & Electrical). New York, NY, USA: Elsevier Sci., 2007. [Online]. Available: https://books.google.com/books?id=b5S0JqHMoxAC

[29] M. Cantono, J. L. Auge, and V. Curri, "Modelling the impact of SRS on NLI generation in commercial equipment: An experimental investigation," in *Proc. Opt. Fiber Commun. Conf.*, 2018, Paper M1D.2. [Online]. Available: http://www.osapublishing.org/abstract.cfm?URI=OFC-2018-M1D.2

[30] M. Cantono *et al.*, "On the interplay of nonlinear interference generation with stimulated Raman scattering for QoT estimation," *J. Lightw. Technol.*, vol. 36, no. 15, pp. 3131–3141, Aug. 2018. [Online]. Available: http://jlt.osa.org/abstract.cfm?URI=jlt-36-15-3131

[31] D. J. Elson *et al.*, "Investigation of bandwidth loading in optical fibre transmission using amplified spontaneous emission noise," *Opt. Exp.*, vol. 25, no. 16, pp. 19529–19537, Aug. 2017. [Online]. Available: http://www.opticsexpress.org/abstract.cfm?URI=oe-25-16-19529

[32] "Characteristics of a single-mode optical fibre and cable," ITU-T Recommendation G.652, Nov. 2016. [Online]. Available: http://handle.itu.int/11.1002/1000/13076

[33] "Characteristics of a non-zero dispersion-shifted single-mode optical fibre and cable," ITU-T Recommendation G.655, Nov. 2009. [Online]. Available: https://www.itu.int/rec/T-REC-G.655-200911-I/en

[34] V. Curri *et al.*, "Design strategies and merit of system parameters for uniform uncompensated links supporting Nyquist-WDM transmission," *J. Lightw. Technol.*, vol. 33, no. 18, pp. 3921–3932, Sep. 2015.

[35] F. A. Flood, "L-band erbium-doped fiber amplifiers," in *Proc. Opt. Fiber Commun. Conf. Postconf. Ed. Trends Opt. Photon. Vol. 37*, Mar. 2000, vol. 2, pp. 102–104.

[36] A. Mori and Y. Ohishi, "Tellurite-based EDFAs for broadband communication," in *Proc. Opt. Fiber Commun. Conf. Exhib. Conf. Ed.*, Feb. 1998, Paper WA1.

[37] E. Dianov, "Bismuth-doped optical fibers: A challenging active medium for near-IR lasers and optical amplifiers," *Light, Sci. Appl.*, vol. 1, pp. 1–7, May 2012, doi: 10.1038/lsa.2012.12.

[38] H. S. Chung, M. S. Lee, D. Lee, N. Park, and D. J. DiGiovanni, "Low noise, high efficiency l-band EDFA with 980 nm pumping," *Electron. Lett.*, vol. 35, no. 13, pp. 1099–1100, Jun. 1999.

[39] J. Lee, U.-C. Ryu, S. J. Ahn, and N. Park, "Enhancement of power conversion efficiency for an l-band EDFA with a secondary pumping effect in the unpumped EDF section," *IEEE Photon. Technol. Lett.*, vol. 11, no. 1, pp. 42–44, Jan. 1999.

[40] J. Renaudier *et al.*, "107 Tb/s transmission of 103-nm bandwidth over 3×100 km SSMF using ultra-wideband hybrid Raman/SOA repeaters," in *Proc. Opt. Fiber Commun. Conf.*, 2019, Paper Tu3F.2. [Online]. Available: http://www.osapublishing.org/abstract.cfm?URI=OFC-2019-Tu3F.2

[41] H. Masuda, *Hybrid EDFA/Raman Amplifiers*. New York, NY, USA: Springer, 2004, pp. 413–443. [Online]. Available: https://doi.org/10.1007/978-0-387-21585-3_4

[42] V. Curri and A. Carena, "Merit of Raman pumping in uniform and uncompensated links supporting NyWDM transmission," *J. Lightw. Technol.*, vol. 34, no. 2, pp. 554–565, Jan. 2016.

[43] J. Bromage, "Raman amplification for fiber communications systems," *J. Lightw. Technol.*, vol. 22, no. 1, pp. 79–93, Jan. 2004.

[44] S. Namiki and Y. Emori, "Ultrabroad-band Raman amplifiers pumped and gain-equalized by wavelength-division-multiplexed high-power laser diodes," *IEEE J. Sel. Topics Quantum Electron.*, vol. 7, no. 1, pp. 3–16, Jan. 2001.

[45] C. R. S. Fludger, V. Handerek, and R. J. Mears, "Fundamental noise limits in broadband Raman amplifiers," in *Proc. Opt. Fiber Commun. Conf. Exhib. Tech. Dig. Postconf. Ed.*, Mar. 2001, vol. 1, Paper MA5.

[46] S. Kado, Y. Emori, and S. Namiki, "Gain and noise tilt control in multi-wavelength bi-directionally pumped Raman amplifier," in *Proc. Opt. Fiber Commun. Conf. Exhib.*, Mar. 2002, pp. 62–63.

[47] P. M. Krummrich, R. E. Neuhauser, and C. Glingener, "Bandwidth limitations of broadband distributed Raman fiber amplifiers for WDM systems," in *Proc. Opt. Fiber Commun. Conf. Exhib. Postconf. Ed.*, Mar. 2001, vol. 1, Paper MI3.

[48] T.-T. Kung, C.-T. Chang, J.-C. Dung, and S. Chi, "Four-wave mixing between pump and signal in a distributed Raman amplifier," *J. Lightw. Technol.*, vol. 21, no. 5, pp. 1164–1170, May 2003.

[49] J.-C. Bouteiller, L. Leng, and C. Headley, "Pump-pump four-wave mixing in distributed Raman amplified systems," *J. Lightw. Technol.*, vol. 22, no. 3, pp. 723–732, Mar. 2004.

[50] S. D. Emami *et al.*, "Micro-bending based optical band-pass filter and its application in S-band thulium-doped fiber amplifier," *Opt. Exp.*, vol. 20, no. 28, pp. 29784–29797, Dec. 2012. [Online]. Available: http://www.opticsexpress.org/abstract.cfm?URI=oe-20-28-29784

[51] J. A. Jay, "An overview of macrobending and microbending of optical fibers," White Paper, Corning Inc., Corning, NY, USA, 2010.

[52] Y. Yamamoto, Y. Kawaguchi, and M. Hirano, "Low-loss and low-nonlinearity pure-silica-core fiber for C- and L-band broadband transmission," *J. Lightw. Technol.*, vol. 34, no. 2, pp. 321–326, Jan. 2016.

[53] A. Bononi, P. Serena, N. Rossi, E. Grellier, and F. Vacondio, "Modeling nonlinearity in coherent transmissions with dominant intrachannel-four-wave-mixing," *Opt. Exp.*, vol. 20, no. 7, pp. 7777–7791, Mar. 2012. [Online]. Available: http://www.opticsexpress.org/abstract.cfm?URI=oe-20-7-7777

[54] A. Carena, V. Curri, G. Bosco, P. Poggiolini, and F. Forghieri, "Modeling of the impact of nonlinear propagation effects in uncompensated optical coherent transmission links," *J. Lightw. Technol.*, vol. 30, no. 10, pp. 1524–1539, May 2012.

[55] D. Semrau, R. I. Killey, and P. Bayvel, "A closed-form approximation of the Gaussian noise model in the presence of inter-channel stimulated Raman scattering," *J. Lightw. Technol.*, vol. 37, no. 9, pp. 1924–1936, May 2019.

[56] P. Poggiolini *et al.*, "The LOGON strategy for low-complexity control plane implementation in new-generation flexible networks," in *Proc. Opt. Fiber Commun. Conf. Expo./Nat. Fiber Opt. Eng. Conf.*, Mar. 2013, Paper OW1H.3.

[57] M. Filer, M. Cantono, A. Ferrari, G. Grammel, G. Galimberti, and V. Curri, "Multi-vendor experimental validation of an open source QoT estimator for optical networks," *J. Lightw. Technol.*, vol. 36, no. 15, pp. 3073–3082, Aug. 2018. [Online]. Available: http://jlt.osa.org/abstract.cfm?URI=jlt-36-15-3073

[58] A. Carena, V. Curri, R. Gaudino, P. Poggiolini, and S. Benedetto, "A time-domain optical transmission system simulation package accounting for nonlinear and polarization-related effects in fiber," *IEEE J. Sel. Areas Commun.*, vol. 15, no. 4, pp. 751–765, May 1997.

[59] D. J. Ives, P. Bayvel, and S. J. Savory, "Adapting transmitter power and modulation format to improve optical network performance utilizing the Gaussian noise model of nonlinear impairments," *J. Lightw. Technol.*, vol. 32, no. 21, pp. 3485–3494, Nov. 2014. [Online]. Available: http://jlt.osa.org/abstract.cfm?URI=jlt-32-21-3485

[60] I. Roberts, J. M. Kahn, and D. Boertjes, "Convex channel power optimization in nonlinear WDM systems using Gaussian noise model," *J. Lightw. Technol.*, vol. 34, no. 13, pp. 3212–3222, Jul. 2016.

[61] C. E. Shannon, "A mathematical theory of communication," *Bell Syst. Tech. J.*, vol. 27, no. 3, pp. 379–423, 1948.

[62] J. M. Cioffi, "Lecture notes in EE 379B—Digital communication II: Coding," Feb. 2005. [Online]. Available: https://web.stanford.edu/group/cioffi/doc/book/chap8.pdf

[63] E. Breverman, N. El-Sakkary, T. Hofmeister, S. Ngai, A. Shaikh, and V. Vusirikala, "Optical zero touch networking—A large operator perspective," in *Proc. Opt. Fiber Commun. Conf.*, 2019, Paper W3G.4. [Online]. Available: http://www.osapublishing.org/abstract.cfm?URI=OFC-2019-W3G.4